University of Science and Technology Houari Boumediène

FACULTY OF PHYSICS

Department of Radiation Physics

Subject:

Beam shaping assembly optimization for boron Neutron Capture Therapy (BNCT)

By
Lilia ZAIDI *

) Director and co-director Thesis : Prof. Mohamed Belgaid, Pr   Sergey Taskaev

(The resume of thesis)

Table des matières

Summary

The objective of our thesis is to model and optimize an irradiation device, which allows to deliver a therapeutic neutron beam suitable for the treatment of deep seated tumors, thus allow treatment without surgery, as part of the BNCT (Boron Neutron Capture Therapy) technique . In order to provide a therapeutic neutron beam, which meets the IAEA's recommendations in terms of quality and intensity, the irradiation device, called BSA (Beam shaping assembly) should be installed between the neutron source and the patient's irradiation point , thus transforming the primary neutron beam into a therapeutic beam .

The BSA consists of a moderator, a reflector, a collimator, a gamma filter and a thermal neutron filter [1] . The nuclear properties of the various components have been studied and discussed. In the quest for an optimum BSA, several BSA configurations based on the specifications of the primary neutron source were designed using the MCNP code.

To evaluate the impact of the beam produced by the optimized BSA in the human body, the Snyder head ghost was used and in-ghost parameters were calculated. We have considered a proton energy of 2.3 MeV, a current of 10 mA and boron concentrations in the tumor, healthy tissues and skin of 52.5 ppm, 15 ppm and 22.5 ppm, respectively. In this study we adopted a limit of exposure to healthy tissue at a maximum point dose equivalent of 11 RBE-Gy, and a maximum skin dose of 16.7 RBE-Gy and an average dose of the brain limited to 7 RBE-Gy, in accordance to the dosimetric limits prescribed in the literature [9] [10] .

The optimal configuration of the designed BSA is used to deliver an average dose of 56.5 Gy may be delivered to the tumor within 40 min irradiation time, wherein the therapeutic ratio is 5.38.

I.   Introduction

Boron Neutron Capture Therapy (BNCT) is a radiotherapy that uses the [10] B nuclide with a high capture cross-section at low energies [2]. This capture reaction, followed by disintegration, can result in high energy deposition in the vicinity of the reaction site. If the boron is selectively introduced into the tumor cells, it is possible to destroy the tumor and save the surrounding healthy tissues because the products of the reaction : Li and He are characterized by a high LET (Linear Energy Transfer), and their range in the tissues is similar to the diameter of the cell. He has a LET of about 150 keV μ m^{-1} and ^{7}Li with a LET of 175 keV μ m^{-1}, the range of these particles are about 10 μm and 4.5 μm , respectively [3] . This offers the ability to target tumor cells and destroy only with high efficiency while sparing other tissues containing less boron-10. Such radiation therapy at the cellular level can provide an extremely accurate dose delivery for effectively treating tumors and reducing side effects. It also has the potential to successfully treat the types of cancer that are truly incurable. However, the success of the BNCT is not guaranteed. It depends on two conditions:

-       the preferential absorption of boron atoms in each cancer cell and

-       delivering a high fluence of thermal neutrons into the target volume.

The goal of our thesis is to deliver a therapeutic neutron beam suitable for the treatment of cancers seated in depth.

Two different neutron beams are commonly used for BNCT: the thermal neutron beam that limits treatment to shallow tumors, such as cutaneous melanoma, and the epithermal neutron beam, harder (0,5 eV<E<10keV) for deep tumors such as glioblastoma multiforme. The latter is the most adequate in our case because it can penetrate deeper into the tissues because of its high energy and can reach the range of thermal energy after being slowed down by the tissues, thus allow treatment without surgery.

In this thesis, after studying the neutron sources that can be used for BNCT, the ^{7}Li(p,n)^{7}Be reaction was chosen because of the high neutron yield with relatively low energy at low incident proton energy. The solid lithium target [4] and the vacuum insulation tandem accelerator (VITA) [5] were considered as neutron source for the BNCT.
The MCNP code [6] based on the Monte Carlo method, applied to many fields of science, including neutron and gamma transport in the materials, is used. The different components of the BSA has been discussed and optimized; the parameters in the air have been checked, and the in-phantom parameters have been calculated. The optimal configuration was chosen in way that the tumors could be treated in the widest possible depth and during the shortest treatment time with a better therapeutic ratio.

II.   Neutron beam design for deep tumors

Optimizing a neutron beam for BNCT, which must be less contaminated and sufficiently intense in accordance with the recommendations of the IAEA [7], is a delicate process. Unlike

X-rays, a few processes can only generate neutrons, and each of them generates neutrons over a large spectrum of energy. Moderation of these neutrons to the appropriate energy range inevitably leads to a significant loss of intensity, sometimes to such a low level that it is therapeutically unacceptable. In addition, most neutron absorbers produce significant contamination by high energy gamma radiation, which is sometimes intolerable.

II. 1 General properties of the irradiation beam

The two main characteristics of the beam of interest are intensity and quality. The intensity of the beam will be the main determinant of the treatment time. The quality of the beam relates to the types, energies and relative intensities of all the radiations present, accompanying the therapeutic beam.

II. 1. 1 Energy range

For BNCT, the thermal neutron beam must be created in the tumor cells in a prescribed target volume. For target volumes well below the surface, epithermal beams will generally be effective. A Previous study shows that it is necessary to provide neutrons with energy distribution reaching a peak of about 10 keV for the irradiation of deep-seated tumors. For this purpose, the recommended energy range is between 0.5 eV and 10 KeV [8].

II. 1. 2 Intensity of the beam

The present experiment shows that the desirable minimum beam intensity would be 10^9 cm^{-2} s^{-1} epithermal neutrons.

II. 1. 3 Quality of the incident beam

The beam quality is determined by four parameters in the air defined by the IAEA.

II. 1. 3.1. The fast neutron component

In BNCT, fast neutrons are with energies higher than 10keV. These neutrons produce protons with high LET in a nonselective process. Therefore, it is necessary to reduce as much as possible the fast neutrons from the incident beam.

Another major objective is clearly to have an epithermal flow as high as possible. The ratio of useful neutrons and the fast neutron dose should be kept below 2.5x10^{-13} Gy cm^2 per epithermal neutron.

II. 1. 3. 2. The gamma radiation component

A non-selective gamma dose is delivered to both tumor tissue and a large volume of healthy tissue. So, it is recommended to eliminate gamma rays from the incident beam. A maximum dose in air is limited to 2x10^{-13} Gy cm^2 per epithermal neutron.

II. 1. 3. 3 The relationship between thermal flux and epithermal flux:

To reduce damage to the scalp or the skin, thermal neutrons in the incident beam must be minimized. The ratio of thermal flux to epithermal flux should be 0.05.

II. 1. 3. 4 The ratio of total neutron current to total neutron flux

This report provides a measure of the fraction of neutrons moving in the forward direction of the beam. A high value is important to limit the divergence of the neutron beam and thus reduce the undesirable irradiation of other tissues. This factor is estimated to be at least 0.7.

III. Neutrons production system

The Neutron sources that can be used in BNCT are various, namely the source of Californium, nuclear reactor, neutron generator, particle accelerator ... etc.

Nowadays, the number of centers dedicated to the BNCT continues to grow. Since accelerators are advantageous than nuclear reactors, in our work, the accelerator at BINP was considered for the optimization of the BSA.

III. 1 source of neutron

For accelerators, endothermic nuclear reacti $^7Li(p, n)^7Be$, $^9Be(p, n)^9B$, $^9Be(d, n)^{10}B$ and $^{12}C(d, n)^{13}N$ are the most used for BNCT. They are attractive in view of the high neutron yield and their energy spectrum, which is low at threshold reactions. Among these reactions, it seems that the reaction $^7Li(p, n)^7Be$ is the best choice in terms of the number of neutrons as well as their energies [11].

IV. The design of the irradiation device

A typical BSA includes a moderator to moderate fast neutrons, a reflector to reduce neutron leakage from the device, a collimator to focus neutrons on the patient's position, the gamma filter, and the thermal neutron filter to minimize unwanted doses.

IV.1 Design and optimization methodology

The design of the entire device includes :

1) Study of the nuclear properties of the nuclei, which can be used as component of the device.
2) Selection of the preliminary materials for the moderator, the reflector, the thermal neutron absorber and the gamma filter, according to their nuclear properties ;
3) Design of a simple BSA's geometry, material of moderation to be use and the other components are added and tested.
4) A comparison of parameters in-air performed for all materials and several possible configurations.
5) Once this step is completed, the geometry and dimension of each component of the BSA are refined for an optimal configuration according to the FOM (reference values).

IV. 1. 1 Moderator

The neutrons emitted by the source (Li, p) belong to the fast neutron energy range, so they can not be used directly. To reduce their energy, we explored different materials by cross section analysis and then by a series of MC calculations.

- Selection of moderator material

Taking into account that our objective is to obtain an epithermal flux, our moderator will be used to slow the fast neutrons of energy higher than 10 KeV towards the epithermal ones. The atoms composing the material must have a high scatering cross section at fast energies, and the smallest possible in the epithermal range. To avoid loss of neutron density and high gamma contamination, the absorption cross section should be as small as possible. In addition, the distance between the neutron source and the output of the epithermal neutron beam must be as short as possible (since the flux varies in $1/r^2$).

To estimate the suitability of the moderator materials, the following quantities were analyzed :
1. The microscopic cross section of neutrons scattering σ_s.
2. The microscopic cross section of neutron absorption σ_a.
3. the "logarithmic mean energy decrement of collision " ξ . This is the average energy lost by a neutron in a collision with a nuclide. It is given by :

$$\mathcal{U} = \ln\left(\frac{E_0}{E_1}\right)$$

Where E_0 and E_1 are the neutron energies before and after collision, respectively. For elastic scattering, the ratio E_0 and E_1 is independent from the initial energy of the neutron, but depends on the atomic mass A of the moderator and the diffusion angle, the relation of $\frac{E_0}{E_1}$ is given by :

$$\frac{E_0}{E_1} = \frac{1}{2}[(1+\alpha)(1-\alpha)\cos\theta]$$

Where $\alpha = [(A - 1) / (A + 1)]^2$.
By averaging on the set of possible values of the diffusion angle θ, one obtains the average logarithmic decrement of the energy, which is only function of the atomic mass of the Moderator

$$\xi = 1 + \alpha / (1 - \alpha) \ln (\alpha)$$

Using ξ , we can calculate the average number of collisions (designated by ♯) necessary to convert an initial energy neutron E_0 to an energy neutron E_1 and this by the following relation:

$$♯ = \ln (E1 / E2) / \xi$$

4. Moderation Power (MP). The effectiveness of a moderator in the deceleration of neutrons depends not only on the value of ξ but also on the probability per unit of traveled distance, between two elastic collisions expressed by the macroscopic scattering cross section Σ_s . The moderation power MP is defined as follows:

$$MP = \xi \, \Sigma_s$$

It is used to compare the moderation efficiency of the considered materials.

5. Moderation Ratio (RM), which is a measure of the effectiveness of moderation without absorption. A great moderating power is necessary for a good moderator, however, a material with great moderating power that has a high absorption cross-section could not be considered good because it would actually reduce neutron energy, but the fraction of surviving neutrons could be too small.

The moderation report is defined as follows :

$$MR = \frac{\xi \, \Sigma_s}{\Sigma_a}$$

IV. 1. 2 Reflector

The neutrons produced have an anisotropic distribution in direction and energy. For this purpose, a reflector is used to minimize the neutron losses due to leakage of neutrons through surfaces other than the irradiation one.

The material with the most appropriate reflector component should have the same characteristics as a moderator (in terms of absorption, slowdown of fast neutrons), except that it should have an elastic scattering which ensures reflection of epithermal neutrons. in a short distance without degrading their energies. We have studied several materials, we can mention: BeO , Be, Al_2O_3, MgO , in addition to the usual materials reported in previous studies : iron and graphite [12], [13].

IV. 1. 3 Collimator

To minimize damage to healthy tissue near the tumor, we need greater beam convergence. The variation of beam divergence is measured by the factor J/ϕ, such that J is the neutron current flowing through the exit surface of the irradiation beam and ϕ is the flux. J/ϕ estimate the directivity of the beam. It is zero when the beam is isotropic and equal to one when it is parallel.

In order to increase the convergence of the beam, a collimator was added to the configuration, where the thickness, shape and composition were optimized.

IV. 1. 4 Filters

The last step, filters for absorption, diffusion of thermal neutrons, fast neutrons and gamma rays are explored. Materials such as Ti, Fe, ^{32}S have been tested for fast neutron contamination and Li-poly, LiF, Pb, Bi for shielding.

V. Results and discussions

V.1 protons on lithium

the reaction ^{7}Li(p, n)^{7}Be has a threshold energy at 1.88 MeV and shows a resonance peak at 2.25 MeV with a cross section of 580 mb, see FIG. 1 obtained from the database EXFOR [14]. Since the increase in the cross-section of the response to proton energies just above the threshold is drastic, a significant source of relatively low energy neutrons are produced.
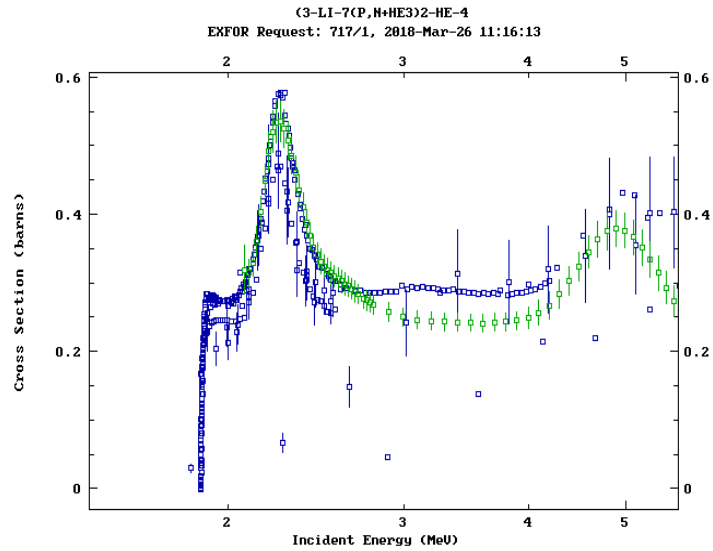
Fig.1 : section efficace de la réaction des protons sur le lithium-7 ^{7}Li (p, n) ^{7}Be.

V.1.1 Choice of proton energy

The increase of the proton energy increase in the neutron yield, but also the neutron spectra become more energetic, as shown in Fig. 2 , where the yield and the maximum energy of the resulting neutrons are expressed as a function of the incident proton beam energy.

We chosed the energy of the 2.3 MeV bombardment protons in order to take advantage of the resonance 7Li (p, n) 7Be reaction at 2.25 MeV. Moreover, this proton energy produce high neutron yields when the beam slows in the thick lithium target (576 n / pC), it may be enough to generate a sufficient amount of epithermal neutrons suitable for treatment. However, the maximum and average neutron energies are 573.1 keV and 233.1 keV, respectively, and therefore require significant moderation to reduce neutron energies to the epithermal region.
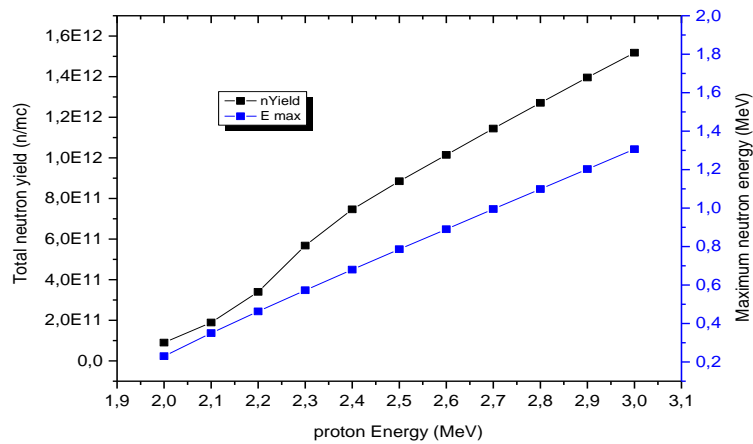
Fig.2 **:** Neutron yield and the maximum energy of the resulting neutrons for the reaction of ⁷ Li (p, n),
depending on the energy of the protons.

V.1.2 Energy spectrum and angular distribution of neutrons

To calculate the angular and energetic dependence of neutrons emitted from the reaction
of 2.3 MeV protons on a solid lithium-7 target, we used the code DROSG-2000 [15] . Yields,
energies, double differential yield per solid angle and neutron energy were calculated.
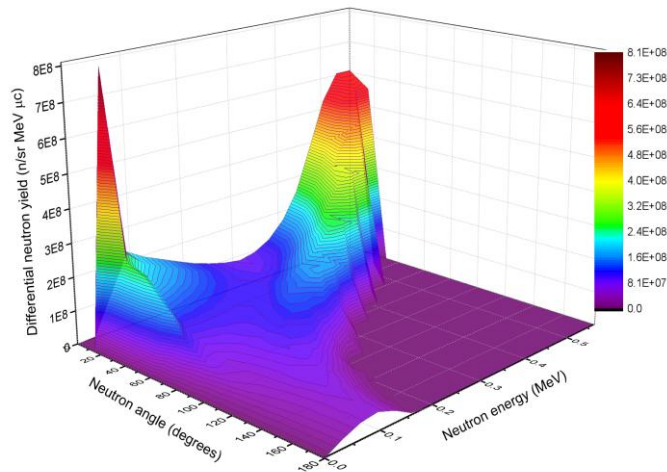
Fig.3 **:** differential neutrons yield for protons energy of 2.3 MeV on a thick target lithium-7.

The Fig 4 shows a neutron yield percentage of the histogram in directions, integrated
on increments of 15 ° beam angle. The results show that 42% of neutrons are emitted between
0 ° and 45 °, 35% neutrons are emitted between 45 ° and 90 °, and 23% of the neutrons
are emitted towards the backward hemisphere.

11
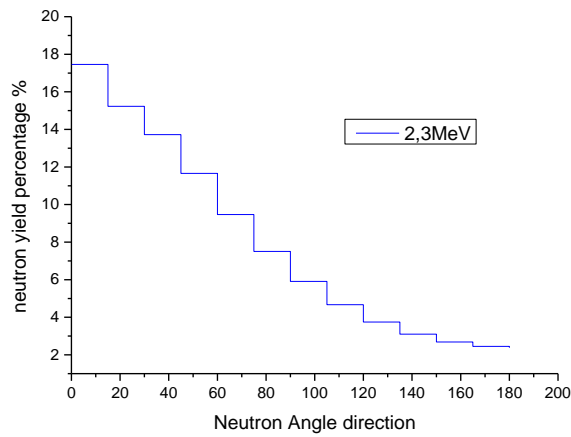
Fig. 4 : Histogram of neutron yield percentage as a function of scattering angle.

The neutron groups described in Fig5 shows that the emission whose neutron group is forward has energies between 100 and 568 keV, the group of 45 ° to 90 ° are energies between 30KeV and 473 keV, and back-directed neutrons have energies
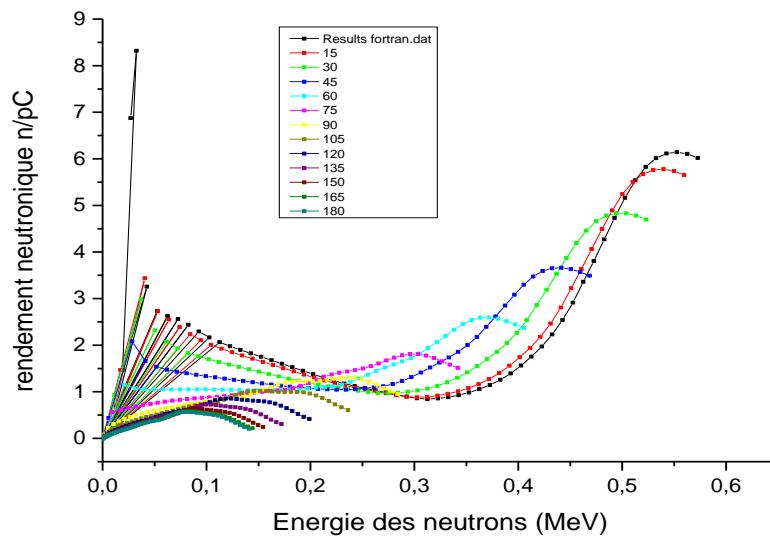
Fig.5 : energy distribution of neutrons according to scattering angles.

The maximum energy of these neutrons is 573 keV and the average energy is 233 keV. The total neutron yield, Y_n , is 576 n / pC , or 9.265×10^{-5} n per proton incident. For a 10 mA proton beam, the total amount of neutrons is $5.78 \times 10^{+12}$ per second.

In the design studies reported in this thesis, source neutrons with their spatial and energy distributions between 0 ° -180 ° degrees are considered in the MCNP simulations. Despite the low rate of neutrons emitted in the opposite direction - a probability of 23% of emission between 90 ° and 180 ° against 77% between 0 ° and 90 °- can contribute to the fluence at irradiation point, and it is also important when shielding calculations are performed.

The definition of angular and energetic distribution was made for each degree. These are introduced into the MCNP SDEF cards for source definition. The distributions were interpolated linearly between the 13 defined points, from 0 to 180 degrees of neutron angular and energy distributions.

V.2 Thickness of the target and gamma radiation production

V.2 .1 Gamma radiation production

Gamma products include   :

1) 478 keV gamma from the inelastic scattering of protons (p, p'γ) and,
2) 14 to 18 MeV gammas from radiative capture (p,γ).

Gammas of inelastic scattering are produced for proton energies above 550 keV. Our lithium target is just thick enough to slow down the proton beam to the threshold energy, so that gamma yields of 478 KeV are reduced significantly. The deposited energy of the remaining protons will be in the support material of the lithium target. The latter must absorb the protons without significant production of gamma radiation [17] [5].

V.2.2 Thickness of the target

The lithium target should be just thick enough to slow down the proton beam at the threshold energy of the reaction (p, n). In this way, there will be no loss of neutron yield, but the gamma yield is significantly reduced.

Using SRIM, the stopping power of the protons in the lithium target was calculated. The scope of the protons in the lithium target as a function of energy is shown in Fig 6.

Fi.6 : the range of protons in Li solid target.

So, in our case, for a 2.3 MeV proton energy, if we consider a thick target, the gamma yield compared to the neutron yield is 0.504 this factor is reduced to 0.234 when we consider a thin target.

V.3 Design of the BSA

V.3.1 The moderator

Selection of materials for the moderator   :

After analysis of scattering cross section of the elements H, D, Be, C, O, Mg, Al, Pb, it is found that the cross sections of the fluorine, magnesium, deuterium and oxygen is about the same for neutrons with energy below 20 KeV, while it represents a series of resonances at energies above 20 KeV, mainly for Mg, F and Al.

Now if we take into account the atomic combinations of materials, their densities and the macroscopic Σ_s diffusion and Σ_a absorption cross sections. The table below Tab1 contains the average energy logarithmic decrement of the neutron collision (ξ) and the average number of collisions ($\sharp$). The figure Fig. 10 shows the energy dependencies of the moderating power of these materials.

Table. 1 . The average logarithmic energy loss and density of materials.

Material	H_2O	D_2O	MgF_2	AlF_3	BeO	Be	C	MgO	Pb	Al2O3
Density g.cm $^{-3}$	1	1.11	3.177	2.88	3.01	1848	2267	3.58	11.35	
Av. Log.E. loss (ξ)	0.707	0.524	0.098	0.098	0,175	0,230	0.158	0,101	0,018	0.1009
$\sharp$ ($E_1 = 300KeV$ and $E_2 = 1KeV$)	19.652	21.092	58.956	59.656	36.157	24,761	36.153	58.957	309.908	60.076
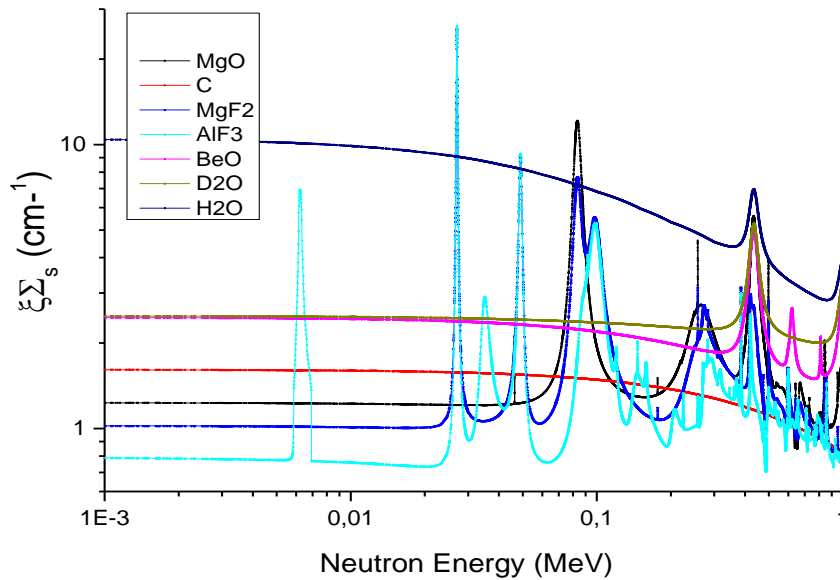
Fig.10 : Power of moderation for materials.

One of the attractive characteristics of aluminum is that it is almost transparent for energy neutrons less than 30 KeV, the disadvantage is that the aluminum with the highest absorption of neutrons, after H. Al is easily activated by neutrons, followed by gamma emissions of high energies.

As the mass numbers of the magnesium and aluminum are close to each other, the values of the log mean energy loss ξ are also close, they are 0.081 for magnesium and 0.072 for aluminum.
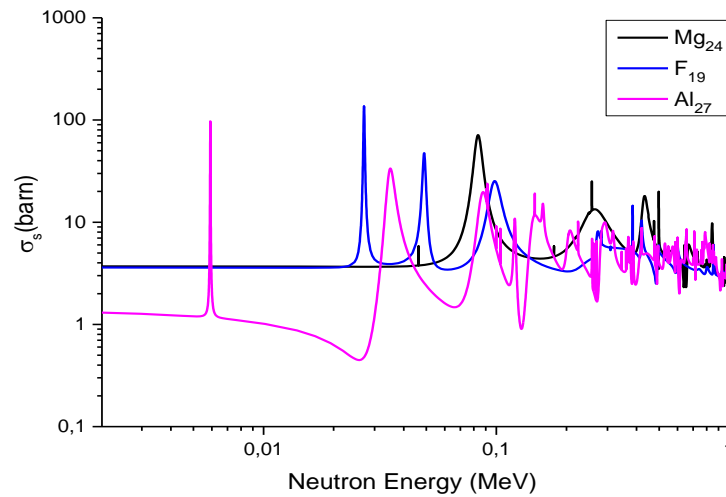
Fig.11: microscopic cross section of diffusion of elements Mg_{24}, F_{19} and Al_{27}.

Fluorine has a minimal radiative capture (comparing to Al and Mg) and whose diffusion properties are comparable to those of Mg, in addition it is the only compound that has an inelastic diffusion at energies below 1MeV, which ensures fast deceleration at energies of 200 keV. Consequently, it would be advantageous to use a compound whose fluorine concentration (weighting) is higher.

Table Tab2 [18] reports the density of fluorides and the concentration of fluorine nuclei in them.

For a proton energy of 2.3 MeV on lithium target, AlF_3 and MgF_2 are considered as potential moderating materials for the treatment of deep tumors by the BNCT, the moderating power of these two elements are presented in Fig13 .

15
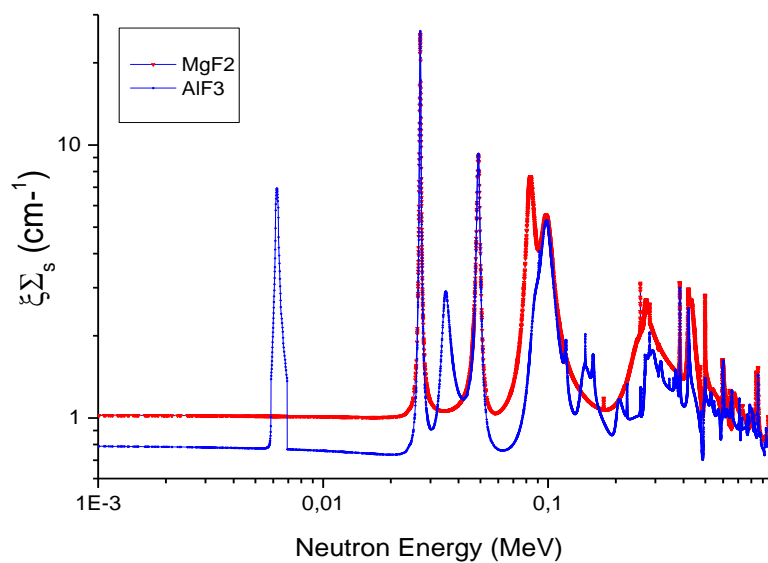
FIG. 13 : Moderation power of MgF_2 and AlF_3 .

Table. 2. Density of fluorides and the concentration of fluorine nuclei in them (Zaidi et al., 2017).

	Density, $g\,cm^{-3}$	Concentration of fluorine nuclei, 10^{22} cm^{-3}
Magnesium fluoride MgF_2	3.177	6.14
Aluminum fluoride AlF_3	2.88	6.19
Lithium fluoride LiF	2.639	6.13
Calcium fluoride CaF_2	3.18	4.90
Fluoroplastic C_2F_4	2.2	5.29

III.2.1 Modeling the moderator

As a first phase, a Monte Carlo calculations was performed for the target-moderator assembly . To estimate the variation of the components of the neutron flux as a function of the height of the moderator, we calculated the average of each one on a surface of a disc of 10cm of diameter at 1cm of the exit of the BSA. Figure 14 shows flux reports: The epithermal/thermal flux ($\varphi_{épith}/\varphi_{ther}$) and epithermal/fast flux ($\varphi_{épith}/_{rap}\varphi$) as a function of the thickness of moderator. It can be noted that the useful flux becomes greater beyond 18cm when a moderator in MgF_2 is used, and from 30cm for AlF_3. On the other hand, the thermal flux is very small comparing to the epithermal flux for the two materials.
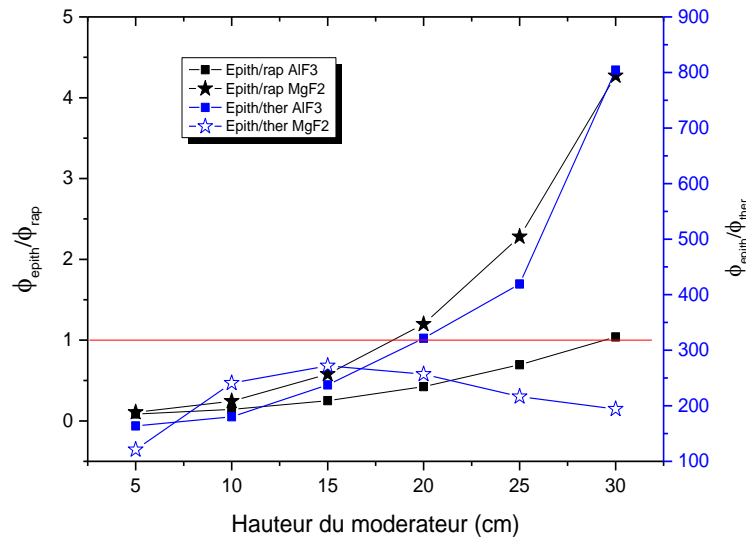
Fig.14 : flux reports based on the height of the moderator.

It can be noted that the intensity of fast neutrons decreases more rapidly in the case of MgF_2 than AlF_3. In contrast, the flux of epithermal neutrons are constantly growing, the maximum intensity is reached at approximately 20cm.

For a thickness of 20cm, the first phase of the design study, the epithermal flux is about 5.08 E^{-5} neutrons/cm^2 for the AlF$_3$ moderator, and 7.93 E^{-5} for MgF$_2$. On the other hand, the intensity of the fast flux is 79% lower for MgF$_2$, (MgF$_2$ 6.618E^{5}n/cm^2 and AlF$_3$ 1.19E^{-4} n/cm^2).
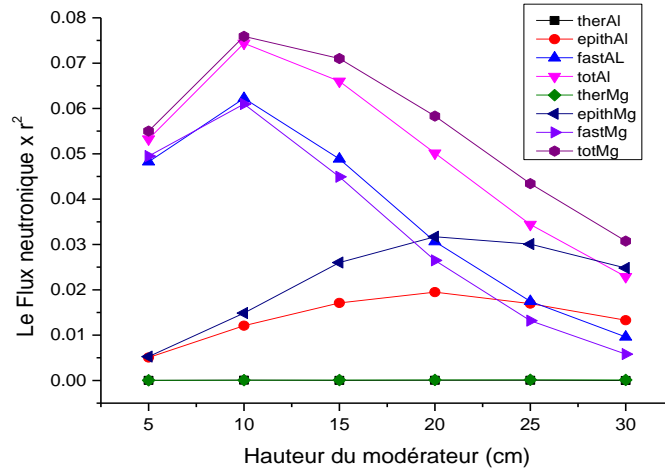
Fig.15 *:* flux versus moderator height.

III.3 Reflector

As a next step, Be, BeO, Al2O3, MgO, C and Pb were tested for the reflector of the front part. The variation of the neutron flux corresponding to the different thicknesses of the reflector for each element calculated at the exit side of the BSA, are calculated. We have also analyzed the ratio of the flux of epithermal / thermal neutrons (ϕ_{ear} / ϕ_{ther}) and the ratio of the flux of epithermal / fast neutrons (ϕ_{ear} /ϕ_{rap}). It has been shown that the appropriate reflector for our configuration is 20 cm MgO.
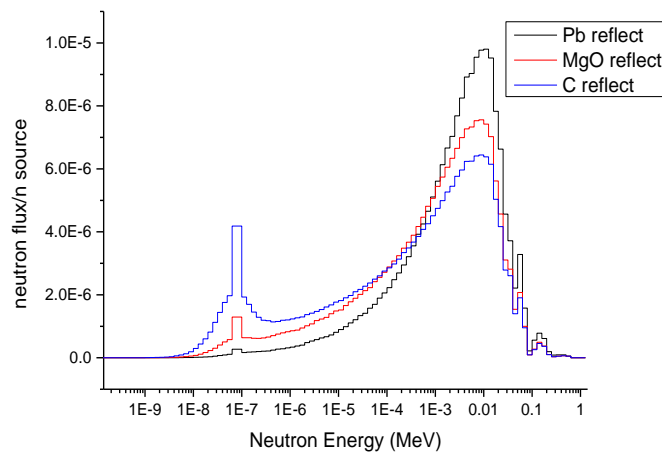
Fig.16 : The neutron flux of Pb reflectors, MgO, C for a thickness of 20cm.

III.4 Collimator and filters

Close to the moderator, we contracted the BSA beam orifice on a circular surface 10 cm in diameter surrounded by the reflector.

III.4.1 Filters

To avoid undesirable thermal neutron contamination, polyethylene-Li and LiF enriched with ^{6}Li were tested.
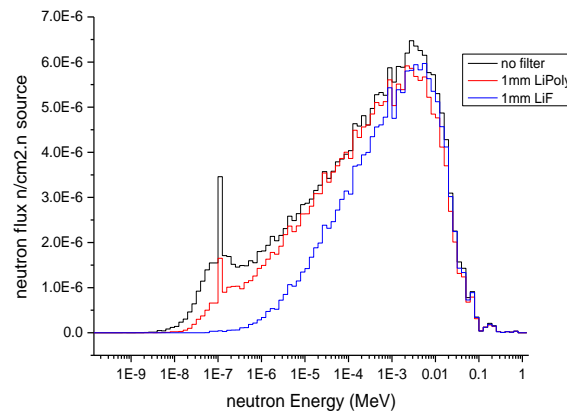
Fig.17 : Flux at the output of the BSA according to the filters and their filter thicknesses.

To avoid undesirable thermal neutron and gamma ray contamination in the beam, a 1mm Bi layer and 1mm Li-polyethylene enriched ^{6}Li were chosen to cover the collimator.

III.4.2 Collimator

In addition to the materials composing the beam orifice, a conical collimator shape and a simple cylindrical of different dimensions were tested.
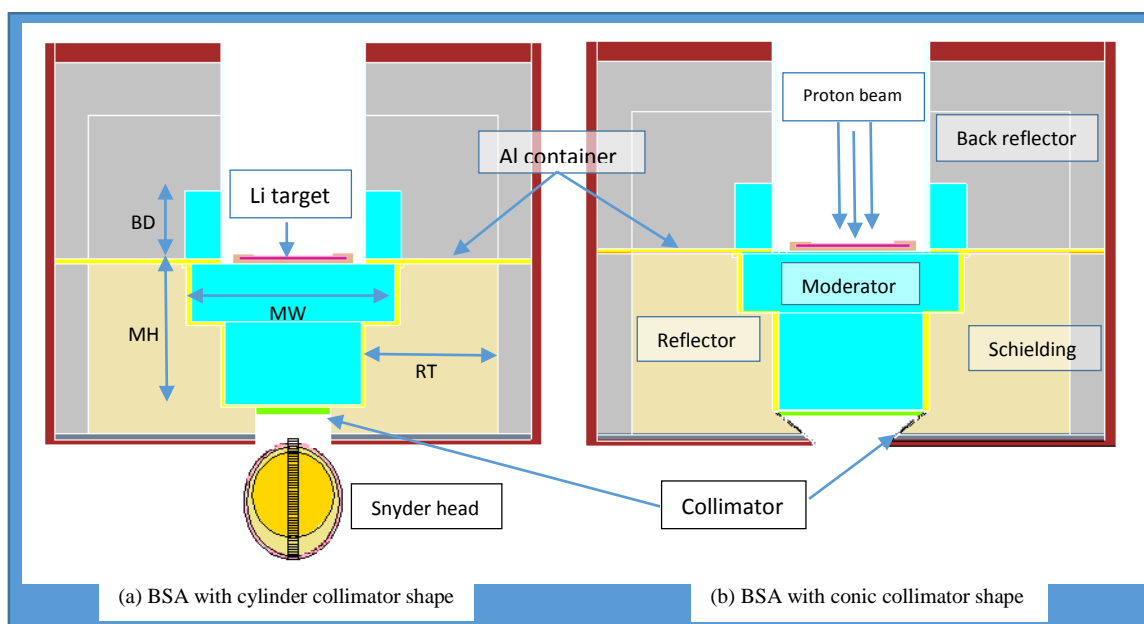
Fig. 18 Cross sectional view of the BSA designed configurations.

In our case, we found that for 5.8 cm collimator size is enough and it is better to use a cylindrical shape because we have less contamination in fast neutrons and thermal neutrons. In addition, the ratio (J / Φ) is a little lower in the case of the conical collimator. By adding the collimator, the ratio J / Φ of the BSA is increased from 0.617 to 0.657.

The radial distributions of thermal, epithermal and fast components fluxes at the exit side of the BSA as a function of the distance from the irradiation axis, are calculated with and without collimator and are presented in FIG.19 .

(a) total neutron flux.   (b) Gamma flux
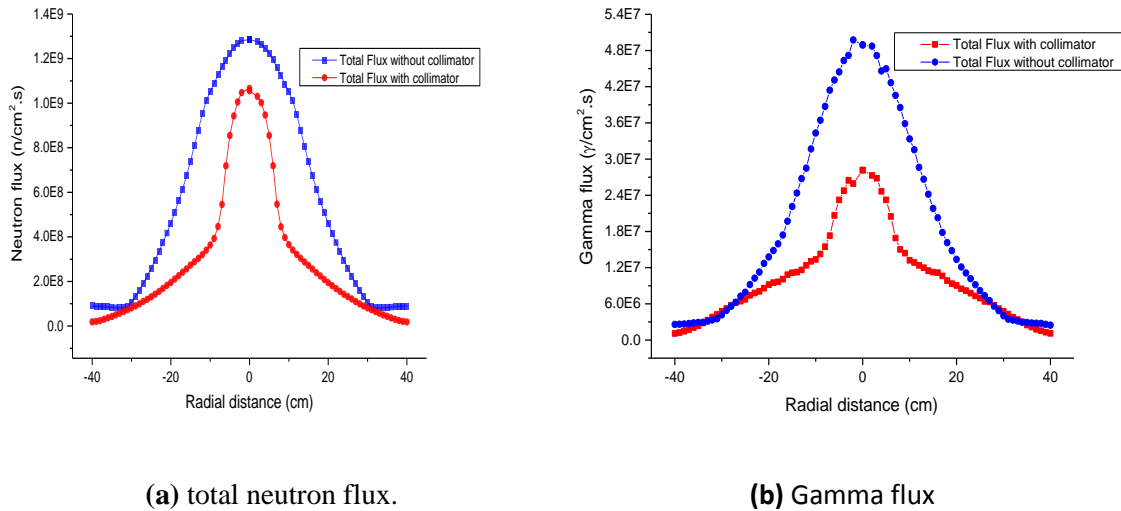
FIG.19 : Comparison of the total flux at the exit of the BSA with a cylindrical collimator and without, as a function of the distance from the irradiation axis.

III.5 Evaluation of the design

The radiation beam outside the BSA presented in the previous section is a mixed field, neutron-photon. The field's suitability for BNCT for the treatment of deep tumors, in the case of GBMs, was assessed. The first aspect consists of calculating the parameters in-air : neutron fluxes and dose components of fast neutrons and gamma rays and flux ratios. They have been calculated and compared to the criteria established by the IAEA. These parameters were also compared to those published by other researchers. The second aspect is the calculation of the parameters in Phantom; this one will be discussed in the section dedicated to dosimetry.

III.5.1 The final configuration of the optimized BSA

The final BSA (see Fig.20) consists of an MgF_2 moderator surrounded by an MgO reflector. An outer layer of polyethylene-lithium and lead protects thermal neutrons and gamma rays, respectively. The 10 cm diameter irradiation port has a 1 cm Ti layer, a 1 mm Bi layer and 1 mm polyethylene-Li to avoid unwanted contamination of fast neutrons, thermal neutrons and gamma rays in the beam.
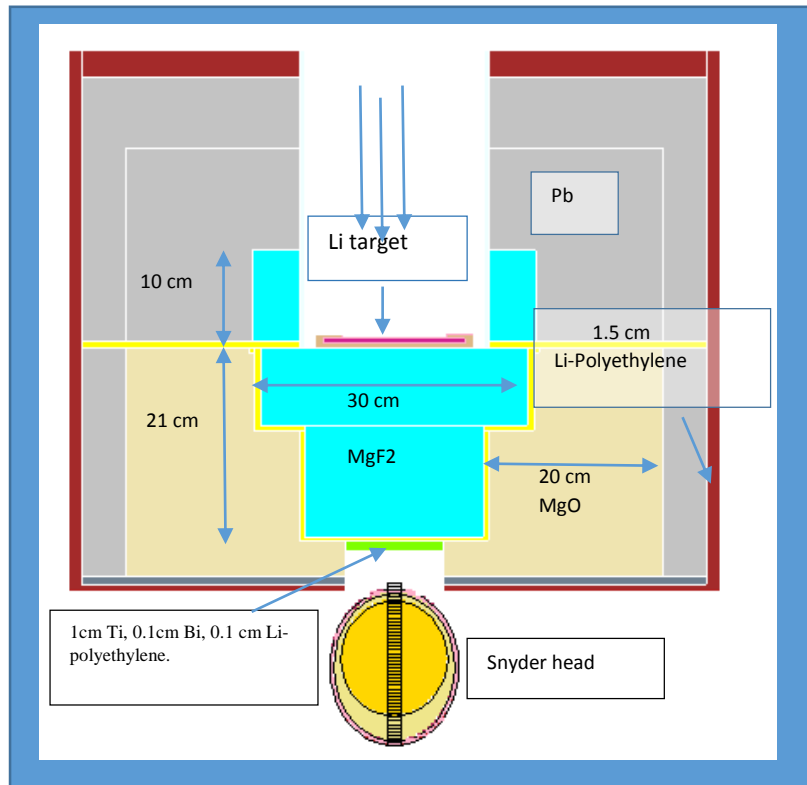
Fig. 20: The final designed BSA.

Figure 21 shows the neutron energy spectrum corresponding to optimal BSA. The generated beam consists of an epithermal neutron flux at 85.1%, where the undesirable dose of undesired neutrons per epithermal neutron is $1.16E^{-14}$ Gy.cm^2 and the corresponding gamma contamination is $1.87E^{-13}$ Gycm^2.
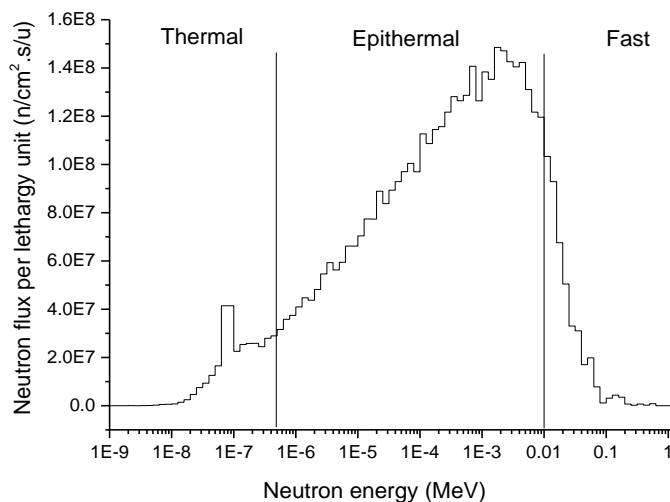
Fig. 21 : Neutron spectrum at beam port of the optimized BSA.

III.5.2 the parameters in the air

Table 3 shows the parameters in the air obtained in our study compared to those published from some BNCT facilities, which are based on a proton accelerator or a reactor.

Table. 3. Beam parameters of our BSA configuration and some published works.

Beam parameters	Neutron yield $(\times 10^{14}$ n/s)	ϕepi $(\times 10^9$ n/cm^2 s)	Dfn/ϕepi $(\times 10^{-13}$ Gy.cm^2)	Dg/ϕepi $(\times 10^{-13}$ Gy.cm^2)	ϕepi/ϕthermal	J/ϕ
IAEA criteria	–	(0.5–1)	<2	<2	>20	>0.7
Our work	5.78E-2	1.04	1.25	1.89	29.4	0.657
Cerullo et al., 2004	4	2.51	3.45	0.21	114.5	0.57
[19]	1.45	4.43	0.59	1.98	121.2	0.61
[20]	–	0.819	7.98	1.18	–	–

IV. dosimetry

The optimized BSA assembly was also evaluated by the in-Phantom distribution of neutron fluxes and doses of various components in the Snyder head phantom, and also by the parameters in the phantom.

IV.3 Parameter evaluation in the ghost

IV.3.1 Profile of neutron flux in Phantom:

The top of the phantom of the head is at the point of irradiation and the center line of the phantom is collinear with the centerline of the BSA.

Figure 21 shows the neutron flux profiles of the three groups (thermal, epithermal and fast) as a function of depth along the central axis of the phantom. We can notice that neutron flux at the surface are dominated by epithermal neutrons. The thermal neutron flux reaches a peak between 2.7 cm and 3.5 cm and decreases rapidly past 4 cm, to be attenuated at a depth of 12 cm inside the phantom.

IV.3.2 Dose profile in Phantom

There are five important components of the absorbed dose in BNCT:
The absorbed dose due to the reaction ^{10}B (n, a)^{7}Li, three components of the absorbed dose due to neutrons interacting with the elements present in the patient's tissue and the absorbed dose due to gamma rays accompanying the beam neutrons. The three components of the absorbed dose, due to the neutrons interacting with the elements of the tissue, are a consequence of the reactions ^{1}H(n, n ')^{1}H, ^{14}N(n, p)^{14}C and ^{1}H(n, γ)^{2}H. The ^{1}H(n, n ')^{1}H component of the dose is the most important for fast neutrons (D_f), while the dose components of the ^{14}N(n, p)^{14}C, ^{1}H (n, γ)^{2}H reactions and ^{10}B(n, α)^{7}Li are important for thermal neutrons.

Neutron flux-kerma conversion factors for human brain tissues are obtained from the elementary kerma coefficients of the ICRU report 63 as well as the appropriate mass fractions of each element.
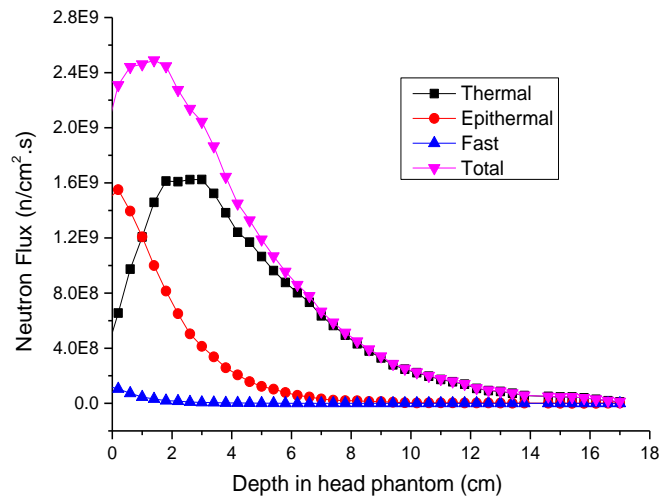
Fig. 21 : Neutron flux profiles in head phantom.
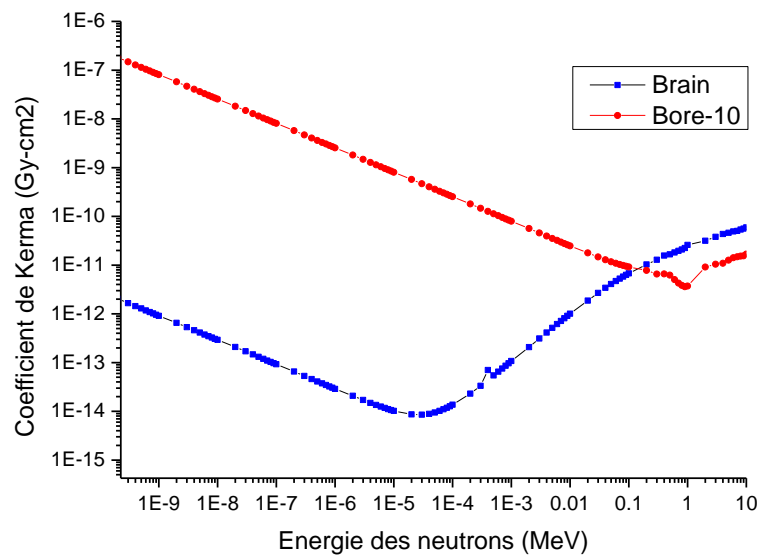
Fig.22 : Flux-KERMA conversion factors for neutrons in tissues and in natural boron with a concentration of 1ppm.

The dose rate (RBEcGy / min) resulting from exposure to epithelial neutrons was calculated using the following formula:

$$D_w = w_\gamma D_\gamma + w_B D_B + w_N D_N + w_{fn} D_{fn} \tag{1}$$

D_w is the weighted total dose, $D\gamma$ is the gamma dose, D_B is the absorbed dose due to boron, D_N is the nitrogen dose and D_{fn} is the fast neutron dose.

The weighting factors are the relative biological effectiveness; they are given in the literature and shown in the table below [21].

Tissue	10B concentration (ppm)	Neutron RBE	10B	γ RBE
Healthy brain	15	3.2	1.35	1
skin	22.5	3.2	2.5	1
tumor	52.5	3.2	3.8	1

IV.3.3 The parameters in Phantom

In the tumor, the AD defined as the maximum depth at which the dose of the tumor exceeds the maximum dose of healthy tissue in our case is equal to 9.7 cm. The treatable depth (TD), corresponding to the maximum depth for which the tumor dose is double value of the healthy tissue dose, is 7.52cm.

To define the total doses, which can be delivered by the BSA, we normalize the doses to the maximum dose of healthy tissue defined at 11 RBE-Gy, because the other dose limits [9] are lower, far to be achieved in our case. Where, the maximum point cutaneous dose and the average brain dose limited to 16.7 RBE-Gy and 7 RBE-Gy, respectively.

After normalizing the doses so that the maximum dose of healthy point tissue was 11RBE-Gy, total tumor dose and healthy tissue profiles were obtained (Figure 13). The normalization factor corresponds to the maximum treatment time of 40 minutes for which an average dose of 2.77 RBE-Gy is administered to the skin with a maximum point dose of 15.58 RBE-Gy and an average of 3.71 RBE.Gy for healthy brain tissue. During this period of irradiation, the average tumor dose of 56.5 RBE-Gy with a minimum tumor dose of 52.2 RBE-Gy can be reached, whereas a therapeutic ratio of tumor to normal tissue is 5,38.
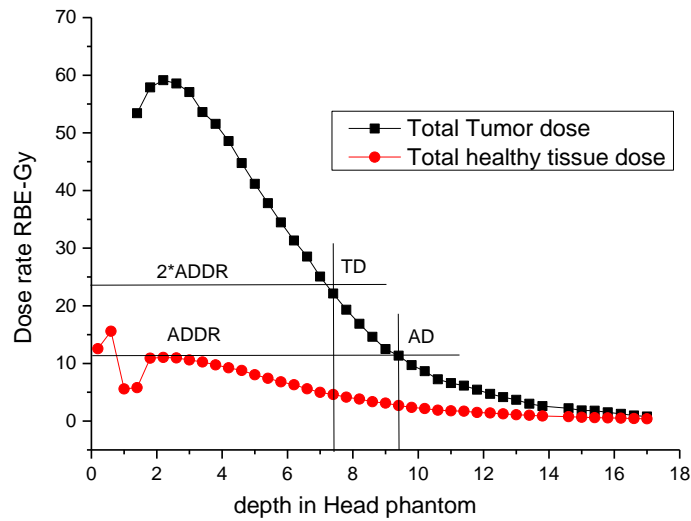
Fig. 23 : Dose profiles in Tumor and Healthy Tissue

Table 4 reports the in-phantom parameters of various published works.

Table. 4. In-phantom parameters of our BSA configuration and some published works.

Facility	ADDR (cGy/min)	AD (cm)	TT (min)	TD (cm)	Tumor: normal tissue 10B concentration (ppm)	Maximum therapeutic ratioTR
Present work , 10mA 2.3 MeV	126.93	9.7	40	7.52	52.5:15	5.38
[12] 30mA, 2.3MeV	–	–	58.6	5.38	52.5:15	–
[22] 10mA,	100	9.1	12.5	–	65:18	–
[19]	41.3	9.4	30.2	7	40:11.42	–
[20]	37.1	8.2	34	6.5	65:18	5.05
THOR	50	8.9	25	5.6	65:18	6

V. Application of MESH tally to dose deposition modeling in the BSA- headconfiguration

We used a MESH tally (grid) to map the deposited energy, the different fluxes (thermal, epithermal, fast neutrons as well as gamma ray flux), and doses in the BSA-Brain configuration.

The superposition of this MESH tally on the geometry of the brain in an XZ plane is illustrated in Figure 24.
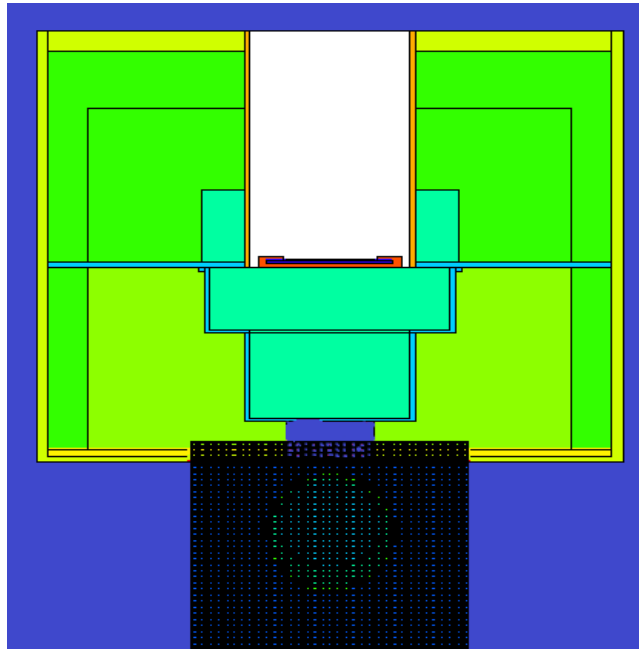
Fig.24: Representation of MESH tally on the brain

Figure 25 shows a longitudinal section in the phantom head of the deposited energy of neutrons (a) and gamma rays (b), where the red and blue colors are respectively representative of the maximum and minimum energy.
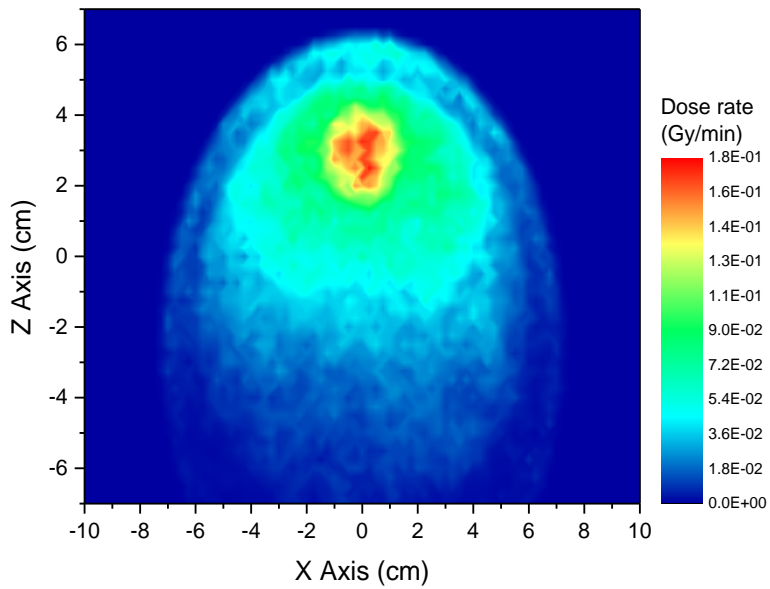
(a)
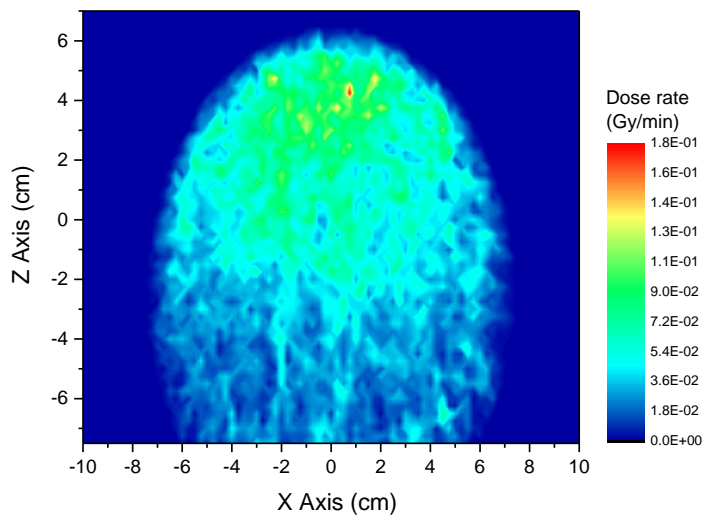
(b)

Fig. 25: Deposited energy of neutrons (a) and gamma rays (b) in the head phantom.

Reference:

[1]   M. Monshizadeh, Y. Kasesaz, H. Khala, and S. Hamidi, "Progress in Nuclear Energy MCNP design of thermal and epithermal neutron beam for BNCT at the Isfahan MNSR," *Prog. Nucl. Energy J.*, vol. 83, pp. 427–432, 2015.

[2]   S. Savolainen, M. Kortesniemi, M. Timonen, H. Koivunoro, T. Seppa, P. Kotiluoto, and 2013. Boron neutron capture therapy (BNCT) in Finland : Technological and physical prospects after 20 years of experiences. doi:10.1016/j.ejmp.2012.04.008 Sere, TomSavolainen, S., Kortesniemi, M., Timonen, M., Koivunoro, H., Seppa, T., Kotiluoto, P., Sere, T., "Boron neutron capture therapy (BNCT) in Finland : Technological and physical prospects after 20 years of experiences," 2013.

[3]   J. Floberg, "The physics of boron neutron capture therapy : an emerging and innovative treatment for glioblastoma and melanoma," 2005.

[4]   B. Bayanov, V. Belov, V. Kindyuk, E. Oparin, and S. Taskaev, "Lithium neutron producing target for BINP accelerator-based neutron source," *Appl. Radiat. Isot.*, vol. 61, pp. 817–821, 2004.

[5]   S. Taskaev, "Accelerator Based Epithermal Neutron Source," *Phys. Part. Nucl.*, vol. 46, no. 6, pp. 956–990, 2015.

[6]   X-5 Monte CarloTeam, "MCNP — A General Monte Carlo N-Particle Transport Code, Version 5," vol. 836. LA-UR-03-1987, 2003.

[7]   IAEA, "Current status of neutron capture therapy," *IAEA-TECDOC-1223*, no. May, 2001.

[8]   T. E. Blue and J. C. Yanch, "Accelerator-based epithermal neutron sources for boron neutron capture therapy of brain tumors," *J. Neurooncol.*, vol. 62, no. 1–2, pp. 19–31,

2003.

[9] M. R. Casal, M. S. Herrera, S. J. González, and D. M. Minsky, "Computational dosimetry of a simulated combined standard X-Rays and BNCT treatment," *Appl. Radiat. Isot.*, vol. 69, no. 12, pp. 1826–1829, 2011.

[10] J. T. Goorley, "Reference Dosimetry Calculations for Neutron Capture Therapy with Comparison of Analytical and Voxel Models," pp. 1–51, 2001.

[11] B. Bayanov, V. Belov, and S. Taskaev, "Neutron producing target for accelerator based neutron," *EPS Euroconference XIX Nucl. Phys. Div. Conf.*, vol. 41, pp. 460–465, 2006.

[12] D. M. Minsky and A. J. Kreiner, "Beam shaping assembly optimization for 7Li(p,n)7Be accelerator based BNCT.," *Appl. Radiat. Isot.*, vol. 88, pp. 233–7, 2014.

[13] C. N. Culbertson, S. Green, A. J. Mason, D. Picton, G. Baugh, R. P. Hugtenburg, Z. Yin, M. C. Scott, and J. M. Nelson, "In-phantom characterisation studies at the Birmingham Accelerator-Generated epIthermal Neutron Source," *Appl. Radiat. Isot.*, vol. 61, no. 969, pp. 733–738, 2004.

[14] IAEA, "EXFOR_ Experimental Nuclear Reaction Data," 2018. [Online]. Available: https://www-nds.iaea.org/exfor/exfor.htm.

[15] M. Drosg, "DROSG-2000:Neutron Source Reactions," *IAEA-NDS-87*, vol. Rev. 9, 2005.

[16] C. L. Lee, X. L. Zhou, R. J. Kudchadker, F. Harmon, and Y. D. Harker, "A Monte Carlo dosimetry-based evaluation of the 7Li(p,n)7Be reaction near threshold for accelerator boron neutron capture therapy.," *Med. Phys.*, vol. 27, no. 1, pp. 192–202, 2000.

[17] D. Kasatov, A. Makarov, I. Shchudlo, and S. Taskaev, "A study of gamma-ray and neutron radiation in the interaction of a 2MeV proton beam with various materials," *Appl. Radiat. Isot.*, vol. 106, no. October 2017, pp. 38–40, 2015.

[18] L. Zaidi, E. Kashaeva, S. Lezhnin, G. Malyshkin, S. Samarin, S. T, S. Taskaev, and S. Frolov, "Neutron-Beam-Shaping Assembly for Boron Neutron-Capture Therapy," *Phys. At. Nucl.*, vol. 80, no. 1, pp. 60–66, 2017.

[19] F. S. Rasouli, S. F. Masoudi, and Y. Kasesaz, "Annals of Nuclear Energy Design of a model for BSA to meet free beam parameters for BNCT based on multiplier system for D − T neutron source," *Ann. Nucl. Energy*, vol. 39, no. 1, pp. 18–25, 2012.

[20] F. Rahmani and M. Shahriari, "Beam shaping assembly optimization of Linac based BNCT and in-phantom depth dose distribution analysis of brain tumors for verification of a beam model," *Ann. Nucl. Energy*, vol. 38, no. 2–3, pp. 404–409, 2011.

[21] M. S. Herrera, S. J. González, D. M. Minsky, and A. J. Kreiner, "Physica Medica Evaluation of performance of an accelerator-based BNCT facility for the treatment of different tumor targets," *Phys. Medica*, vol. 29, no. 5, pp. 436–446, 2013.

[22] O. E. Kononov, V. N. Kononov, M. V. Bokhovko, V. V. Korobeynikov, A. N. Soloviev, A. S. Sysoev, I. A. Gulidov, W. T. Chu, and D. W. Nigg, "Optimization of an accelerator-based epithermal neutron source for neutron capture therapy," *Appl. Radiat. Isot.*, vol. 61, no. 5, pp. 1009–1013, 2004.

[23] MCNPX^{TM} 2.4.0, "Monte Carlo N-Particle Transport Code System for Multiparticle and High Energy Applications." OAK RIDGE NATIONAL LABORATORY, Los Alamos, New Mexico, 2002.